Improvement of Energy Thresholds for Scintillation Detectors Using a Monolithic 2×2 Multi-Pixel Photon Counter Array with a Coincidence Technique

Takamasa Miura[1]*, Takeshi Nakamori[1], Jun Kataoka[1], Takuya Kato[1], Kenichi Sato[2], Yoshitaka Ishikawa[2], Kazuhisa Yamamura[2], Nobuyuki Kawabata[2]

[1]*Research Institute for Science and Engineering, Waseda University, 3-4-1, Ohkubo, Shinjuku, Tokyo 169-8555*

[2]*Solid State Division, Hamamatsu Photonics K. K., 1126-1, Ichino-cho, Hamamatsu, Shizuoka 435-8558*

The performance of a large-area, monolithic Hamamatsu Multi-Pixel Photon Counter (MPPC) was tested consisting of a 2×2 array of 3×3 mm^2 pixels. MPPC is a novel type of semiconductor photodetector comprising multiple avalanche photodiode (APD) pixels operated in Geiger mode. Despite its great advantage of signal multiplication comparable to that achieved with the photomultiplier tube (PMT), the detection of weak scintillation light signals is quite difficult due to the severe contamination of dark counts, which typically amounts to $\simeq$ 1 Mcps/3×3mm^2 at room temperature. In this study, a coincidence technique was applied for scintillation detectors to improve the detection efficiency for low energy gamma-rays. The detector consisted of a 10×10×10 mm^3 crystals of GSO, BGO and Pr:LuAG optically coupled with the 2×2 MPPC-array. With this technique, we demonstrated that the contamination of dark counts was reduced with a rejection efficiency of more than 99.8 %. As a result, 22.2 keV gamma-rays were successfully detected with a GSO scintillator as measured at +20 °C.

KEYWORDS: gamma-rays, scintillation detector, energy threshold, MPPC, coincidence

1. Introduction

A Multi-Pixel Photon Counter (MPPC), also known as a Silicon Photo-Multiplier (SiPM), is a compact, high performance semiconductor photodetector comprising numerous Geiger mode avalanche photodiode (APD) pixels. In particular, MPPC offers great advantages such as low bias voltage operation (typically ∼70 V), high gain (10^{5-6}) almost comparable to conventional photomultiplier tubes (PMTs) and imperviousness

*E-mail address: miura-tkms.eijo@toki.waseda.jp

to magnetic fields.[1–3] However, one of its weak points is the limited number of pixels, resulting in the nonlinear response of output signals. Each APD pixel has "dead time" (typically $\sim afew10$ nsec) once the Geiger discharge has triggered, namely, where multiple photons entering a single pixel cannot be counted within the dead time. Moreover, thermal electrons also trigger Geiger discharge, resulting in substantial contamination of "dark counts", which typically amounts to 1–4 Mcps for 3×3 mm^2 MPPCs (25μm type) measured at room temperature (+25°C).[1–3] Nevertheless, its compactness and high gain are relatively attractive in various fields of high energy physics. For instance, MPPCs will be implemented as a photo sensor to determine weak scintillation light signals in the T2K experiment in order to measure the neutrino oscillation.[4] The use of compact semiconductor photodetectors like MPPC and APD, rather than traditional PMTs, are also promoted in various other ways as described below.

X-ray and gamma-ray astronomical satellites often carry various scintillators, not only as main detectors but also active shields, which effectively reduce background events caused by charged particles (including geomagnetically trapped particles and primary cosmic rays) as well as atmospheric gamma-rays. For instance, the hard X-ray detector (HXD)[5] onboard Suzaku (launched in 2005)[6] utilizes $Bi_{12}Ge_3O_{20}$ (BGO) crystals as the active shield for a phoswich detector. 36 PMTs were implemented in the HXD, but semiconductor photodetectors, if applicable, can easily replace such bulky systems by saving *both* space and power. Firmly motivated, a Tokyo Tech pico-satellite, Cute1.7+APD II, validates the inaugural use of APDs as a radiation detector in a space experiment.[7] The Astro-H, which is a Japanese X-ray astronomy satellite alongside Suzaku to be launched in 2014, will carry 68 APDs to read out shield BGO crystals both in the hard X-ray imager (HXI) and soft gamma-ray detector (SGD).[8] These APDs are linear mode devices operating with only a moderate gain of 50−100, thus making it difficult to achieve energy thresholds as low as 50 keV. In this context, MPPC could be a promising device to replace the APD and further extend the energy coverage of scintillation detectors.

Positron Emission Tomography (PET), another good example of MPPC application, is a well-established method for diagnosing locational and active information on cancers within human bodies or in animals.[9] Conventional PET detectors consist of hundreds of PMTs with pixelized inorganic scintillators like $Lu_2(SiO_4)O$ (LSO), $Gd_2(SiO_4)O$ (GSO) and BGO. PET combined with computed tomography (PET/CT) is currently most popular, but CT imaging suffers from poor soft-tissue contrast, with patients also

subjected to a significant radiation dose that exceeds that received from the PET itself. In contrast, magnetic resonance imaging (MRI) offers excellent soft-tissue contrast and anatomical detail without the additional radiation. Unfortunately, PMT is difficult to use within the MRI high magnetic field of $afew$ T, hence efforts to replace the PMT with APD or MPPC have been actively studied in literature.[10,11] Moreover, MPPC offers excellent timing resolution thanks to its high gain. A combination of MPPC with brand-new scintillators with excellent light output and/or fast timing properties is being investigated for future application in a Time-Of-Flight (TOF) PET scanner.[12] Pr-doped $Lu_3Al_5O_{12}$ (Pr:LuAG)[13,14] is one such scintillator characterized by its very rapid decay, high density and high light yield (see Table I). Its performance with UV-enhanced APD array is already reported elsewhere[14] but testing with the MPPC will be described here for the first time.

Dark counts of MPPC can be severely problematic for all applications and hence should be suppressed as far as possible to ensure optimal detector performance. The idea of rejecting > 99 % of dark counts was suggested by R.Bencardino, et al.,[15] featuring an anti-coincidence technique where two MPPCs were stuck to a single plastic scintillator and triggers were generated when both MPPCs fired at the same time. In this paper, a similar but more advanced application was applied using a monolithic, large area 2×2 MPPC array coupled with various scintillators (GSO, BGO and Pr:LuAG) to improve their energy thresholds. It is shown that the contamination of dark counts can be reduced with efficiency exceeding 99.8 %, substantially improving the signal-to-noise ratio for gamma-ray spectroscopies at around a few tens of keV.

2. Basic properties

2.1 2×2 MPPC-array

For this study, the monolithic 2×2 MPPC array S10985-025C from Hamamatsu (Fig. 1) was selected due to its superior pulse linearity and low dark counts rate. Each MPPC pixel was 3×3 mm^2, comprising a 120×120 Geiger mode APD matrix arranged with a pitch of 25 μm. The dark count, Geiger discharge triggered by thermal electrons, of each MPPC pixel (3×3 mm^2) was 1.3 Mcps with a gain of 2.75×10^5 measured at 25 °C. Other basic characteristics of the MPPC array are summarized in Table II.

First, the gain characteristic of each MPPC pixels was measured as a function of bias voltage. The output charges from the MPPC were estimated by the single photoelectron (1p.e.) peak, which were individually taken with the charge sensitive

ADC (HOSHIN V005). The results are shown in Fig. 2 as measured at +20, 0, and −20 °C, respectively. Although the gain curves generally show good linearity within the measured gain of (2−3)×10^5, in the lower bias region, the measured gains are slightly lower than that expected from an extrapolation of the curve determined from the higher bias region (e.g. the curves gradually bend toward less gain below 71.6 V at +20 °C; see Fig. 2(a)). This is because at a low bias voltage, MPPC cannot operate properly due to the Geiger discharge instability. The gain variation among the pixels are only ±2.9 % within the measured range of (2−3)×10^5. This gain variation is defined by ($GAIN_{max}$ – $GAIN_{min}$)/$GAIN_{ave}$, where $GAIN_{max}$, $GAIN_{min}$ and $GAIN_{ave}$ are the maximum, minimum and mean gain among the four pixels. The temperature dependence of the MPPC gain by linear fits to the data above 2×10^5 was estimated and then compared between −20 and +20 °C. It emerged that the bias voltage should be corrected to 56.6 ± 1.1 mV/°C to maintain uniform gain at different temperatures.

Second, the variation of dark counts for individual MPPC pixels was measured, as a function of the pulse height of output signals. The MPPC is operated at +20 °C with a gain of 2.75×10^5. Output signals from the individual MPPC pixels are multiplied by a factor of 100 using a fast current amplifier (Phillips 6954) and fed into discriminators (Technoland N-TM 210V4). Signals from the discriminators are directly counted by visual scalers (Technoland N-OR 425). The variation of count rates is presented in Fig 3 for each MPPC pixel, as a function of the discriminator threshold. It can be seen that the dark counts due to 1 p.e. clearly appear as a plateau between −5 and −10 mV, and its count rate is about 900 kcps, as measured at +20°C.

2.2 Scintillators

In our experiment, GSO, BGO, and Pr:LuAG cubic scintillators of $10 \times 10 \times 10$ mm^3 size were specifically chosen (see Fig 1), to go alongside the MPPC array described above. The basic parameters of each scintillator are summarized in TableI. It is noted that the peak wavelengths of GSO and BGO favor MPPC because the latter is sensitive within the range 350 to 500 nm. Moreover, these scintillators were implemented in the HXD onboard Suzaku as main (GSO) or shield (BGO) detectors (see §1). In contrast, the short decay time of Pr:LuAG is particularly noteworthy as implemented in future PET scanners (§1) and also beneficial for MPPC to effectively reject dark counts as it facilitates a substantially narrow gate width as described below.

Before testing with 2×2 MPPC-array, the performance of each of the cubic scintilla-

tors was tested using traditional PMT (Hamamatsu R7899-MOD1(EG)) as a reference. Each scintillator was coated with a Teflon tape and silicone optical grease (OKEN N6262A) was used for the optical coupling between the PMT and the scintillators. The measurement was operated at 20 °C, and the operation bias of the PMT was set to 1250 V, corresponding to a gain of $afew\ 10^6$. Anode signals were directly fed into the charge sensitive ADC (HOSHIN V005). The gate widths were set to 200 (GSO and Pr:LuAG) and 500 nsec (BGO), respectively. FWHM energy resolutions of 9.1±0.1 (GSO), 14.0±0.1 (BGO), and 12.2±0.3 % (Pr: LuAG) were respectively obtained for 662 keV gamma-rays from ^{137}Cs.

3. Detecting gamma-rays with coincidence technique

The setup of our measurements is initially described, followed by an overview of the system in Fig 4. The MPPC array and the scintillators were optically coupled using silicone optical grease (OKEN N6262A) and a scintillator and MPPC array were wrapped as a whole, using Teflon tape. The output signals from each of the MPPC pixels were multiplied by a factor of 100 using a fast current amplifier (Phillips 6954) and then inverted/divided by Quad linear FAN IN/OUT (Phillips 740). One of the divided signals was directly fed into the charge sensitive ADC (HOSHIN V005) after a 100 nsec delay (using Technoland N-TS 100), whereas another signal was used to make a gate for the ADC. The threshold level of the discriminator (Technoland N-TM 405) was set to 0.5 $\sim$ 1 p.e. level (see also Fig 3), and the output width was set to 75 nsec, the maximum length with this module. Before making the final ADC gate, the coincidence among 1 to 4 MPPC channels was determined using a coincidence module (Kaizu Works KN470), and adjusted by a gate and delay generator (Technoland N-TM 307). A common bias voltage was supplied to each MPPC pixel by KEITHLEY 2400, corresponding to a gain of 2.75×10^5. All the data were taken at +20 °C.

Before taking the data, the ADC gate width was carefully optimized. Apparently, the wider ADC gate can contain a greater fraction of the charge signals from the scintillator, but meanwhile, the increased dark count will contaminate. The signal-to-noise ratio was thus scanned as a function of gate width, before searching for the optimal value allowing the lowest energy threshold when measured with 662 keV gamma-rays. Consequently, it was concluded that the optimal width for the ADC gate should be 200 nsec for GSO and Pr:LuAG, and 500 nsec for the BGO, respectively, as measured at room temperature (+20 °C).

First, details of how effectively the coincidence technique works to reduce the dark counts are presented, by irradiating 60 keV gamma-rays from ^{241}Am on the GSO scintillator. Figure 5 compares the energy spectra taken with various numbers of coincidence channels, from 1 (triggered only by a single channel, i.e. without coincidence) to 4 (coincidence of all channels). A prominent peak at around 5 keV is due to the dark counts. It is apparent that the coincidence technique drastically reduces the dark counts, where the background trigger rate derived from the dark counts decreases from 9.0×10^2 kcps (without the coincidence) to 1.4×10^2, 1.9×10 and 1.7 kcps with 2-, 3-, and 4-fold coincidences, respectively. In particular, when the 4-fold coincidence is applied, the dark count is effectively reduced with an rejection efficiency of > 99.8 %. The energy resolutions for 59.5 keV gamma-rays of each spectrum are 60 ± 3 % (FWHM), where the peak position and energy resolution may not be significantly affected by the dark count contamination.

Next, an energy spectrum of ^{137}Cs was measured using this coincidence technique. The spectra with the GSO are shown in Fig 6, in which the solid and dashed lines represent 4-fold coincidence and no coincidence respectively. The FWHM energy resolutions are both 15.0 ± 0.1 % for 662 keV. With the coincident triggers, as well as 662 keV gamma-rays, the 32 keV K_α X-ray peak could also be very clearly detected, while this low energy peak was heavily diluted by the dark count and inevitably smoothed out without the coincidence technique. The result successfully demonstrates a significant improvement in the signal-to-noise ratio at the lowest energy range of the scintillation detector.

The energy spectra of ^{137}Cs were also measured with the BGO and Pr:LuAG on the 2×2 MPPC array using the coincidence technique. The spectra obtained are shown in Fig 7 with the GSO spectrum for comparison. Although the 32 keV X-ray peak can be identified in the GSO spectrum, neither the BGO spectrum nor Pr:LuAG shows this peak. These results are discussed in the following section. The energy resolutions (FWHM) of 662 keV were 18.4 ± 0.1% (BGO), and 23.8 ± 0.1% (Pr:LuAG).

Finally, 22 keV gamma-rays were measured from ^{109}Cd with the GSO, in which the coincidence technique worked most effectively. The spectra are shown in Fig 8, whereby the solid and dashed lines correspond to the spectrum taken with and without the 4-fold coincidence, respectively. The 22 keV gamma-ray peak was clearly detected by the coincidence and energy resolution of 63 ± 4 % (FWHM). Therefore the energy threshold of the GSO with the MPPC array was proved to be $\simeq$10 keV.

4. Discussion and conclusion

In this study, a coincidence technique with a 2×2 MPPC array was employed and in turn rejection of dark noise is effectively carried out. It was shown that dark counts triggers are suppressed by more than 99.8 %. Consequently, 22.2 keV gamma-rays were successfully detected with the GSO at +20 °C.

Although PMT and MPPC have comparable photon detection efficiency at 440 nm, which is the peak GSO wavelength, the energy resolutions of 662 keV gamma-rays measured with the MPPC were worse than with the PMT. One of the reasons could be the difference in the collection efficiency of the scintillation photons. This is because the MPPC array covers only 6×6 mm^2, while the PMT has a larger window than the face of the crystal of 10×10 mm^2. The number of photoelectrons detected can be calculated using the charges recorded by the ADC and the MPPC gain. The expected number of scintillation photons from Table I is also known, whereupon the ratio of these numbers indicates the "total" photon collection efficiency, which may be a combination of two factors, namely the efficiency of the photon transportation from the crystal to the MPPC and the detection efficiency at the latter. For instance, with the GSO, 490 photoelectrons are detected as opposed to $10^4 \times 0.662 \sim 6.6 \times 10^3$ scintillation photons expected (see Table I). Therefore the total efficiency is estimated as $490/(6.6 \times 10^3) \sim 7.4$ %. The total efficiencies turned out to be much worse in all cases than the detection efficiency of 20 ∼ 25 %. Besides, we defined the energy threshold in the following way. Because 662 keV gamma-rays generated 490 photoelectrons with the GSO, it can be assumed that 1 photoelectron corresponds to 1.35 keV. Thus, with the 4-fold coincidence, the energy threshold corresponds to $1.35 \times 4 = 5.4$ keV of gamma-rays. These numbers are summarized in Table III with the case for the other scintillators.

In the case with the BGO, the 32 keV X-ray peak could hardly be detected, probably because the BGO yielded only ∼ 250 photons by 32 keV X-rays within the decay time of 300 nsec. From the total collection efficiency in Table III, ∼ 4 photoelectrons per MPPC pixel are expected for 32 keV X-rays. Because of the long BGO decay, the gate width should be correspondingly extended, which hampers efforts to exclude dark count contamination.

For the Pr:LuAG, the intrinsic background derived from ^{176}Lu, which emits electrons in beta decay, must be considered, since the spectrum of Pr:LuAG contains not only gamma-ray but also electron background events (see Fig 7). Moreover, the quantity of photoelectrons detected by 662 keV gamma-rays is not comparable to that with

the GSO, though the Pr:LuAG yields more than twice as many photons as the GSO. Accordingly, as with the BGO, 32 keV X-rays could not be detected clearly. The major cause is the fact that the peak wavelength of Pr:LuAG is 310 nm, at which the photon detection efficiency of the MPPC is less than 10 %. In fact, total photon collection efficiency was almost one third of that of the GSO (see Table III). Such disadvantage is mainly due to epoxy resins conventionally used as the window of APDs. Besides, the Teflon tapes are not particularly reflective for UV light, meaning the scintillation light from Pr:LuAG cannot be collected efficiently. Yoshino, et al.[14] developed UV-enhanced APD, which significantly improved the quantum efficiency by ~ 10 times at the Pr:LuAG peak wavelength. We expect the development of UV-enhanced MPPC to achieve much better performances with Pr:LuAG, in term of both energy resolution and lower energy detectability.

Table I. Characteristics of the GSO, BGO,[16–18] and Pr:LuAG[13] scintillators.

	GSO	BGO	Pr:LuAG
Size (mm^3)		$10 \times 10 \times 10$	
Density (g/cm^3)	6.71	7.13	6.73
Light yield (photons/MeV)	1.0×10^4	8.2×10^3	2.0×10^4
Decay time (nsec)	30−60	300	∼20
Peak wavelength (nm)	430	480	310

Table II. Specification of the MPPC array S10985-025C[19] at +25 °C.

Item	Spec
Total active area (mm^2)	6×6
Number of elements	2×2
Pixel size of a Geiger-mode APD (μm^2)	25×25
Number of Geiger-mode APD pixels	14400 ×4
Operation voltage (V)	72.17±0.03
Gain	2.75×10^5
Dark count rate at 0.5 p.e. threshold (Mcps)	1.3 ×4

Table III. Performance of the MPPC array with each scintillator for 662 keV gamma-rays.

	GSO	BGO	Pr:LuAG
The quantity of photoelectrons detected	490	329	259
Total photon collection efficiency[1] (%)	7.4	6.1	2.0
Energy threshold with 4-fold coincidence (keV)	5.4	8.0	10.2

1 The ratio of the quantity of the photoelectrons detected to the number of the photons yielded from the scintillator.

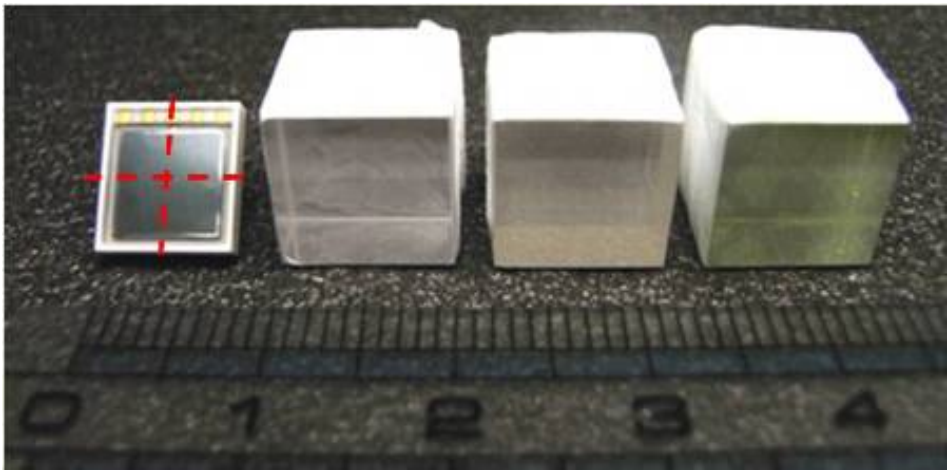

Fig. 1. (Color online)Photograph of the 2×2 MPPC array, the GSO, the BGO and the Pr:LuAG, from left to right. The gaps between each MPPC pixel are illustrated by a red dashed line, and the dimensions of the scintillators are 10×10×10 mm^3.

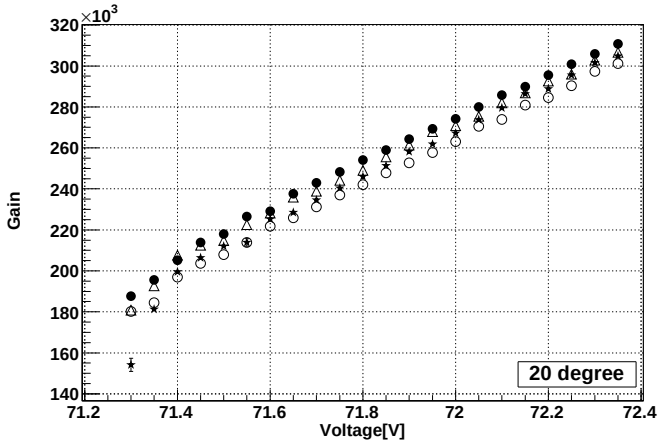

(a)

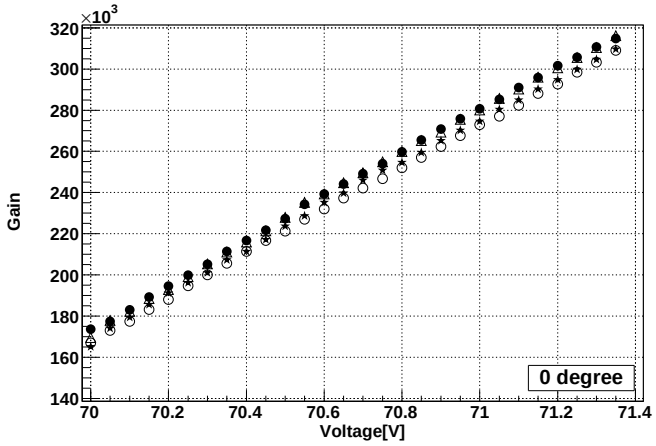

(b)

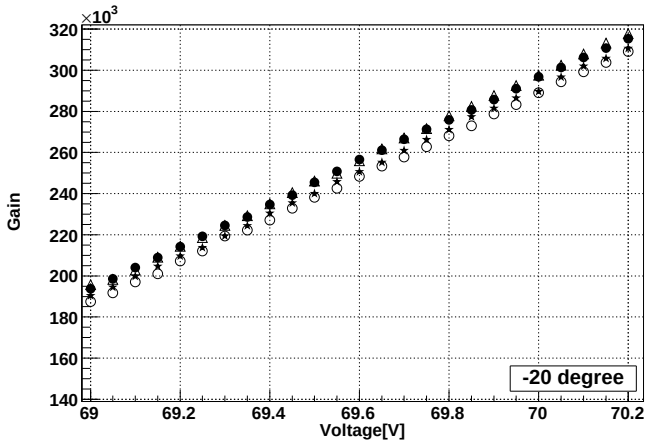

(c)

Fig. 2. Gains of 2×2 MPPC array pixels as a function of bias voltages. The top(a), middle(b) and bottom(c) panels show data measured at +20, 0, and −20 °C, respectively. Filled circles, open circles, triangles and stars correspond to the pixels located in the top left, top right, bottom left and bottom right of Figure 1, respectively.

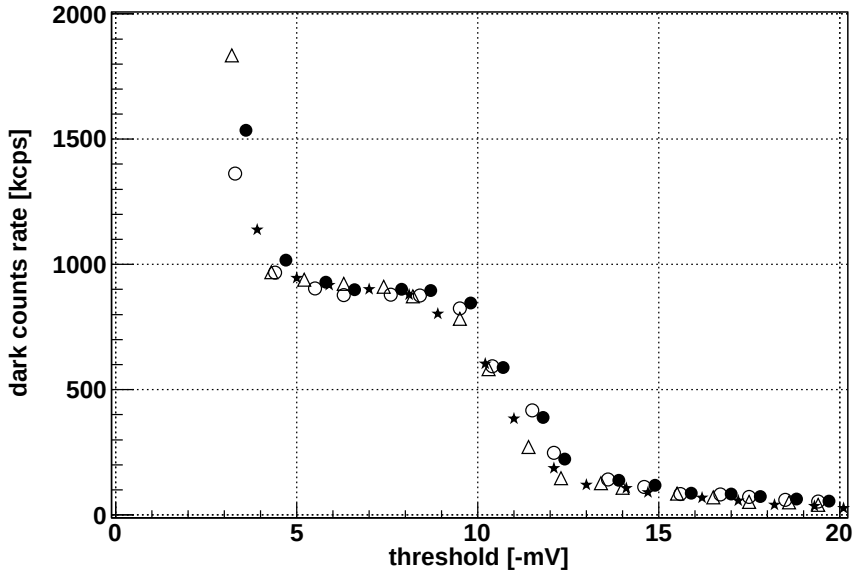

Fig. 3. Dark count rates at +20 °C as a function of the threshold for each MPPC pixel. Filled circles, open circles, triangles and stars correspond to the pixels located in the top left, top right, bottom left and bottom right of Figure 1, respectively.

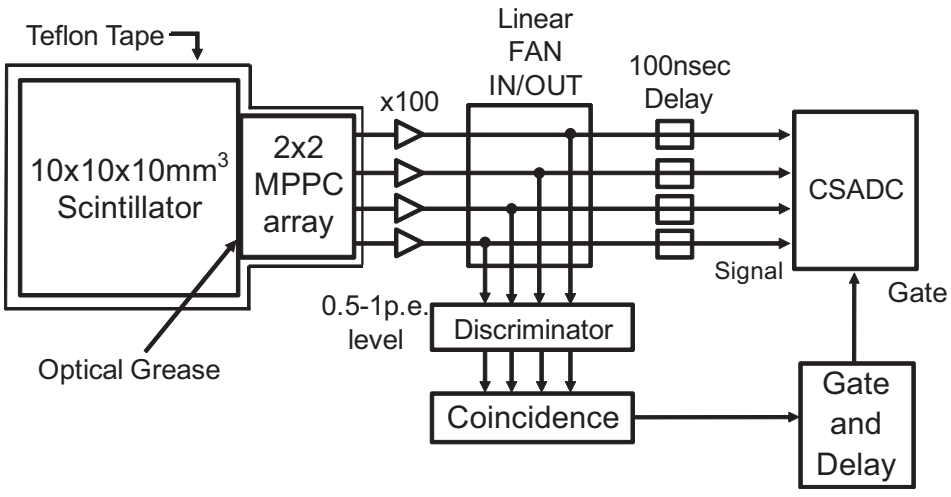

Fig. 4. Diagram of the readout system.

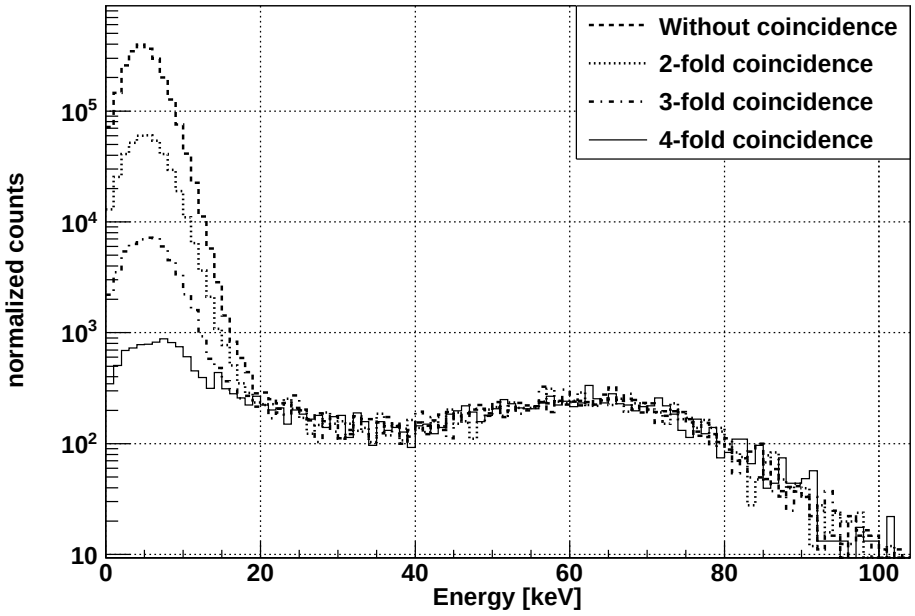

Fig. 5. Energy spectra of the ^{241}Am measured with the GSO at +20 °C for the different trigger conditions (see text). Each spectrum is normalized at the photoelectric absorption peak. The dashed line shows the spectrum without the coincidence trigger while dotted, dot-dashed and solid lines correspond to 2-, 3- and 4-fold coincident events respectively.

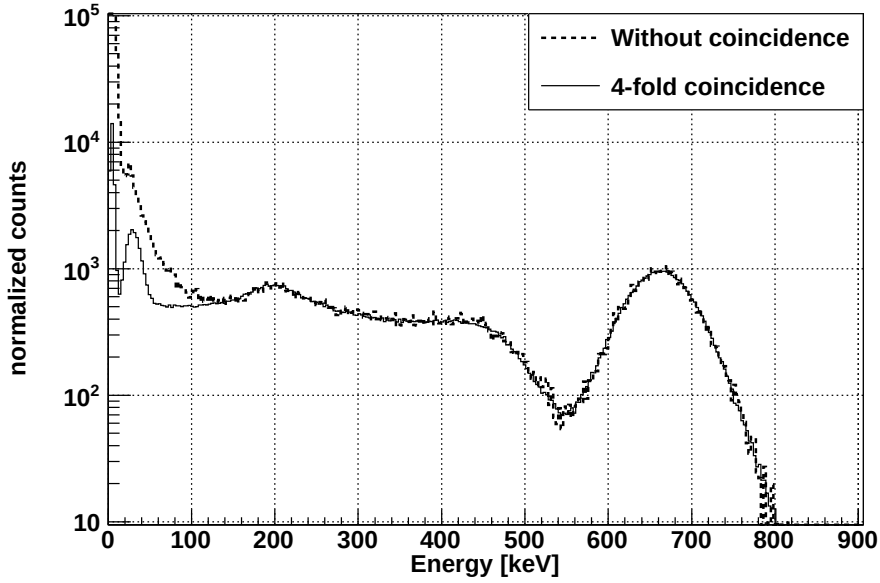

Fig. 6. Energy spectra of ^{137}Cs measured with the GSO at +20 °C. Solid and dashed lines correspond to cases with and without the coincidence respectively.

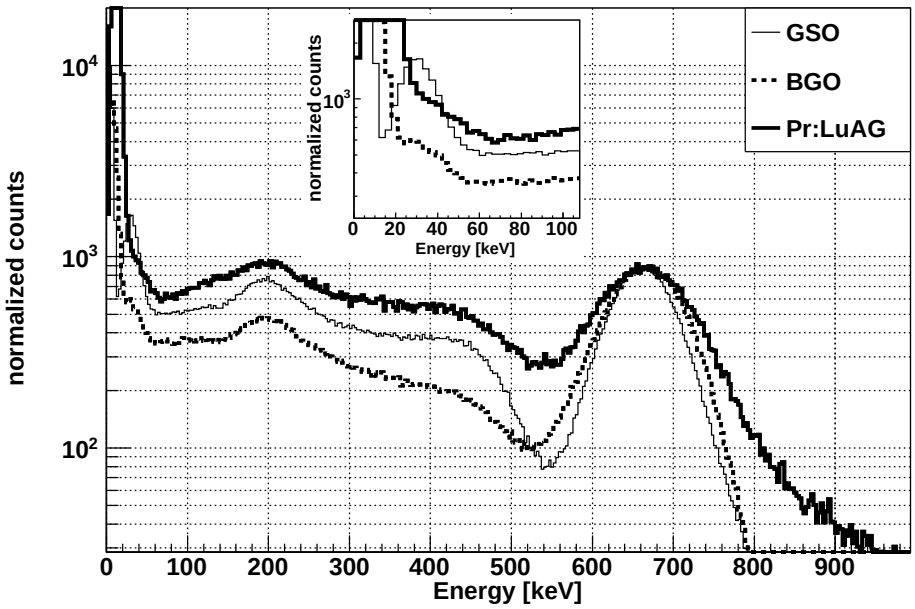

Fig. 7. Energy spectra of ^{137}Cs measured with the three scintillators on 2×2 MPPC array with the 4-fold coincidence. Solid, dashed and thick solid lines represent spectra with GSO, BGO, and Pr:LuAG, respectively. The inset panel is a close-up view around 32 keV peaks.

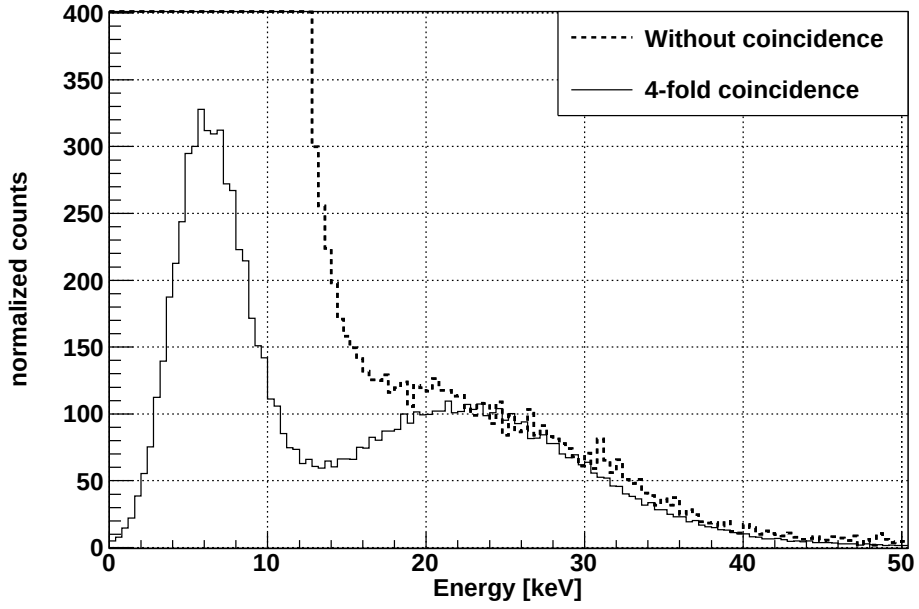

Fig. 8. ^{109}Cd gamma-ray spectra with the GSO at +20 °C. Solid and dashed lines correspond to cases with and without the coincidence respectively.

References

1) S.Gomi, M.Taguchi, H.Hano,S.Itoh, T.Kubota, T.Maeda, Y.Mazuka, H.Otono, E.Sano, Y.Sudo, T.Tsubokawa, M.Yamaoka, H.Yamazaki, S.Uozumi, T.Yoshioka, T.Iijima, K.Kawagoe, S.H.Kim, T,Matsumura, K.Miyabayashi, T.Murakami, T.Nakadaira, T.Nakaya, T.Shinkawa, T.Takeshita, M.Yokoyama, and K.Yoshimura: IEEE Trans. Nucl. Sci. N30-108 (2006) 1105.

2) K.Yamamoto, K.Yamamura, K.Sato, S.Kamakura, T.Ota, H.Suzuki, S.Ohsuka: IEEE Trans. Nucl. Sci. N24-292 (2007) 1511.

3) D.J.Herbert, V.Saveliev, N.Belcari, N.D'Ascenzo, A.D.Guerra, and A.Golovin: IEEE Trans. Nucl. Sci. 53 (2006) 389.

4) A. Vacheret: Nucl. Instrum. Methods Phys. Res., Sect. A 623 (2010) 201.

5) T.Takahashi, K.Abe, M.Endo, Y.Endo, Y.Ezoe, Y.Fukazawa, M.Hamaya, S.Hirakuri, S.Hong, M.Horii, H.Inoue, N.Isobe, T.Itoh, N.Iyomoto, T.Kamae, D.Kasama, J.Kataoka, H.Kato, M.Kawaharada, N.Kawano, K.Kawashima, S.Kawasoe, T.Kishishita, T.Kitaguchi, Y.Kobayashi, M.Kokubun, J.Kotoku, M.Kouda, A.Kubota, G.Madejski, K.Makishima, K.Masukawa, Y.Matsumoto, T.Mitani, R.Miyawaki, T.Mizuno, K.Mori, M.Mori, M.Murashima, T.Murakami, K.Nakazawa, H.Niko, M.Nomachi, Y.Okada, M.Ohno, K.Oonuki, N.Ota, H.Ozawa, G.Sato, S.Shinoda, M.Sugiho, M.Suzuki, K.Taguchi, H.Takahashi, I.Takahashi, S.Takeda, K.Tamura, T.Tamura, T.Tanaka, C.Tanihata, M.Tashiro, Y.Terada, S.Tominaga, Y.Uchiyama, S.Watanabe, K.Yamaoka, T.Yanagida, and D.Yonetoku: Publ. Astro. Soc. J. 59 (2007) 35.

6) K.Mitsuda, M.Bautz, H.Inoue, R.L.Kelly, K.Koyama, H.Kunieda, K.Makishima, Y.Ogawara, R.Petre, T.Takahashi, H.Tsunemi, N.E.White, N.Anabuki, L.Angelini, K.Arnaud, H.Awaki, A.Bamba, K.Boyce, G.V.Brown, K.W.Chan, J.Cottam, T.Dotani, J.Doty, K.Ebisawa, Y.Ezoe, A.C.Fabian, E.Figueroa, R.Fujimoto, Y.Fukazawa, T.Furusho, A.Furuzawa, K.Gendreau, R.E.Griffiths, Y.Haba, K.Hamaguchi, I.Harrus, G.Hasinger, I.Hatsukade, K.Hayashida, P.J.Henry, J.S.Hiraga, S.S.Holt, A.Hornschemeier, J.P.Hughes, U.Hwang, M.Ishida, Y.Ishisaki, N.Isobe, M.ItohN.Iyomoto, S.M.Kahn, T.Kamae, H.Katagiri, J.Kataoka, H.Katayama, N.Kawai, C.Kilbourne, K.Kinugasa, S.Kissel, S.Kitamoto, M.Kohama, T.Kohmura, M.Kokubun, T.Kotani, J.Kotoku, A.kubota, G.M.Madejski, Y.Maeda, F.Makino, A.Markowitz, C.Matsumoto, H.Matsumoto, M.Matsuoka, K.Matsushita,

D.M.Cammon, T.Mihara, K.Misaki, E.Miyata, T.Mizuno, K.Mori, H.Mori, M.Morii, H.Moseley, K.Mukai, H.Murakami, T.Murakami, R.Mushotzky, F.Nagase, M.Namiki, H.Negoro, K.Nakazawa, J.Nousek, T.Okajima, Y.Ogasaka, T.Ohashi, T.Oshima, N.Ota, M.Ozaki, H.Ozawa, A.N.Parmar, W.D.Pence, F.S.Porther, J.N.Reeves, G.R.Ricker, I.Sakurai, W.T.Sanders, A.Senda, P.Serlemitsos, R.Shibata, Y.Soong, R.Smith, M.Suzuki, A.E.szymkowiak, H.Takahashi, T.Tamagawa, K.Tamura, T.Tamura, Y.Tanaka, M.Tashiro, Y.Tawara, Y.Terada, Y.Terashima, H.Tomida, K.Torii, Y.Tsuboi, M.Tsujimoto, T.G.Tsuru, M.J.L.Turner, Yoshihiro.Ueda, S.Ueno, M.Ueno, S.Uno, Y.Urata, S.Watanabe, N.Yamamoto, K.Yamaoka, N.Y.Yamasaki, K.Yamashita, M.Yamauchi, S.Yamauchi, T.Yaqoob, D.Yonetoku, and A.Yoshida: Publ. Astro. Soc. J. 59 (2007) 1.

7) J.Kataoka, T.Toizumi, T.Nakamori, Y.Yatsu, Y.Tsubuku, Y.Kuramoto, T.Enomoto, R.Usui, N.Kawai, H.Ashida, K.Omagari, K.Fujihashi, S.Inagawa, Y.Miura, Y.Konda, N.Miyashita, S.Matsunaga, Y.Ishikawa, Y.Matsunaga, and N.Kawabata: J. Geophys. Res. 115 (2010) A05204.

8) T.Takahashi, K.Mitsuda, R.Kelley, F.Aharonian, F.Akimoto, S.Allen, N.Anabuki, L.Angelini, K.Arnaud, H.Awaki, A.Bamba, N.Bando, M.Bautz, R.Blandford, K.Boyce, G.Brown, M.Chernyakova, P.Coppi, E.Costantini, J.Cottam, J.Crow, J.D.Plaa, C.D.Vries, J-W.D.Herder, M.DiPirro, C.Done, T.Dotani, K.Ebisawa, T.Enoto, Y.Ezoe, A.Fabian, R.Fujimoto, Y.Fukazawa, S.Funk, A.Furuzawa, M.Galeazzi, P.Gandhi, K.Gendreau, K.Gilmore, Y.Haba, K.Hamaguchi, I.Hatsukade, K.Hayashida, J.Hiraga, K.Hirose, A.Hornschemeier, J.Hughes, U.Hwang, R.Iizuka, K.Ishibashi, M.Ishida, K.Ishimura, Y.Ishisaki, N.Isobe, M.Ito, N.Iwata, J.Kaastra, T.Kallman, T.Kamae, H.Katagiri, J.Kataoka, S.Katsuda, M.Kawaharada, N.Kawai, S.Kawasaki, D.Khangaluyan, C.Kilbourne, K.Kinugasa, S.Kitamoto, T.Kitayama, T.Kohmura, M.Kokubun, T.Kosaka, T.Kotania, K.Koyama, A.Kubota, H.Kunied, P.Laurent, F.Lebrun, O.Limousin, M.Loewenstein, K.Long, G.Madejski, Y.Maeda, K.Makishima, M.Markevitch, H.Matsumoto, K.Matsushita, D.McCammon, J.Miller, S.Mineshige, K.Minesugi, T.Miyazawa, T.Mizuno, K.Mori, H.Mori, K.Mukai, H.Murakami, T.Murakami, R.Mushotzky, Y.Nakagawa, T.Nakagawa, H.Nakajima, T.Nakamori, K.Nakazawa, Y.Namba, M.Nomachi, S.Dell, H.Ogawa, M.Ogawa, K.Ogi, T.Ohashi, M.Ohno, M.Ohta, T.Okajim, N.Ota, M.Ozaki, F.Paerels, S.Paltani, A.Parmer, R.Petre, M.Pohl, S.Porter, B.Ramsey, C.Reynolds, S.Sakai, R.Sambrun, G.Sato,

Y.Satoa, P.Serlemitsos, M.Shida, T.Shimada, K.Shinozaki, P.Shirron, R.Smitha, G.Sneiderman, Y.Soong, L.Stawarz, H.Sugita, A.Szymkowiak, H.Tajima, H.Takahashi, Y.Takei, T.Tamagawa, T.Tamura, K.Tamura, T.Tanaka, Y.Tanaka, Y.Tanaka, M.Tashiro, Y.Tawara, Y.Terada, Y.Terashima, F.Tombesi, H.Tomida, M.Tozuka, Y.Tsuboi, M.Tsujimoto, H.Tsunemi, T.Tsurua, H.Uchida, Y.Uchiyama, H.Uchiyama, Y.Ueda, S.Unoa, M.Urry, S.Watanabe, N.White, T.Yamada, H.Yamaguchia, K.Yamaoka, N.Yamasaki, M.Yamauchi, S.Yamauchib, Y.Yatsu, D.Yonetoku, A.Yoshida: Proc. SPIE 7732 (2010) 77320Z-1

9) W.W.Moses: Nucl. Instrum. Methods Phys. Res., Sect. A 471 (2001) 209.

10) J.Kataoka, H.Matsuda, F.Nishikido, M.Koizumi, H.Ikeda, M.Yoshino, T.Miura, S.Tanaka, Y.Ishikawa, N.Kawabata, K.Shimizu, Y.Matsunaga, S.Kishimoto, H.Kubo, Y.Yanagida, and T.Nakamori: IEEE Trans. Nucl. Sci. 57 (2010) 2448.

11) A.Nassalski, M.Moszyński, A.Syntfeld-Każuch, T.Szczęśniak, ŁŚwiderski, D.Wolski, T.Batsch, and J.Baszak: IEEE Trans. Nucl. Sci. 57 (2010) 1008.

12) G.-C.Wang: IEEE Trans. Nucl. Sci. 57 (2010) 25.

13) K.Kamada, T.Yanagida, K.Tsutsumi, Y.Usuki, M.Sato, H.Ogino, A.Novoselov, A.Yoshikawa, M.Kobayashi, S.Sugimoto, and F.Saitoi: IEEE Trans. Nucl. Sci. 56 (2009) 570.

14) M.Yoshino, J.Kataoka, T.Nakamori, H.Matsuda, T.Miura, Y.Ishikawa, N.Kawabata, Y.Matsunaga, K.Kamada, Y.Usuki, A.Yoshikawa, T.Yanagida : to be published in Nucl. Instrum. Methods Phys. Res., Sect. A.

15) R.Bencardino, J.E.Eberhardt, R.Preston: Nucl. Instrum. Methods Phys. Res., Sect. A 619 (2010) 497.

16) E.Sakai: IEEE Trans. Nucl. Sci. NS-34 (1987) 418.

17) I.Holl, E.Lorenz, G.Mageras: IEEE Trans. Nucl. Sci. 35 (1988) 105.

18) H.Ishibashi, K.Shimizu, K.SuSa: IEEE Trans. Nucl. Sci. 36 (1989) 170.

19) Hamamatsu catalog : http://jp.hamamatsu.com/products/sensor−ssd/4010/4025/S10985-025C/index_ja.html